Bioorganic & Medicinal Chemistry 18 (2010) 5063–5070

Contents lists available at ScienceDirect

Bioorganic & Medicinal Chemistry

journal homepage: www.elsevier.com/locate/bmc

# Synthesis, semipreparative HPLC separation, biological evaluation, and 3D-QSAR of hydrazothiazole derivatives as human monoamine oxidase B inhibitors

Franco Chimenti [a], Daniela Secci [a,*], Adriana Bolasco [a], Paola Chimenti [a], Arianna Granese [a], Simone Carradori [a], Elias Maccioni [b], M. Cristina Cardia [b], Matilde Yáñez [c], Francisco Orallo [c], Stefano Alcaro [d], Francesco Ortuso [d], Roberto Cirilli [e], Rosella Ferretti [e], Simona Distinto [d,g], Johannes Kirchmair [f], Thierry Langer [g]

[a] Dipartimento di Chimica e Tecnologie del Farmaco Università degli Studi di Roma 'La Sapienza', P.le A. Moro 5, 00185 Roma, Italy
[b] Dipartimento Farmaco Chimico Tecnologico, Università di Cagliari, Via Ospedale 72, 09124 Cagliari, Italy
[c] Departamento de Farmacología and Instituto de Farmacia Industrial, Facultad de Farmacia, Universidad de Santiago de Compostela, Campus Universitario Sur, E-15782 Santiago de Compostela (La Coruña), Spain
[d] Dipartimento di Scienze Farmaco Biologiche 'Complesso Ninì Barbieri', Università degli Studi di Catanzaro 'Magna Graecia', 88021 Roccelletta di Borgia (CZ), Italy
[e] Istituto Superiore di Sanità, Dipartimento del Farmaco, V.le Regina Elena 299, 00161 Roma, Italy
[f] Department of Pharmaceutical Chemistry, Institute of Pharmacy and Center for Molecular Biosciences (CMBI), University of Innsbruck, Innrain 52, A-6020 Innsbruck, Austria
[g] Inte:Ligand Software-Entwicklungs und Consulting GmbH, Clemens Maria Hofbauer-Gasse 6, A-2344 Maria Enzersdorf, Austria

ARTICLE INFO

*Article history:*
Received 17 March 2010
Revised 25 May 2010
Accepted 26 May 2010
Available online 1 June 2010

*Keywords:*
Hydrazothiazole derivatives
3D-QSAR
Human monoamine oxidase B inhibitors

ABSTRACT

The present study reports on synthesis in high yields (70–99%), HPLC enantioseparation, inhibitory activity against human monoamino oxidases, and molecular modeling including 3D-QSAR studies, of a large series of (4-aryl-thiazol-2-yl)hydrazones (**1**–**45**). Most of the synthesized compounds proved to be potent and selective inhibitors of hMAO-B isoform in the micromolar or nanomolar range, thus demonstrating that hydrazothiazole could be considered a good pharmacophore to design new hMAO-B inhibitors. Due to the presence in some derivatives of a chiral center, we also performed a semipreparative chromatographic enantioseparation of these compounds obtained by a stereoconservative pattern. The separated enantiomers were submitted to in vitro biological evaluation to point out the stereorecognition of the active site of the enzyme towards these structures. Finally, a 3D-QSAR study was carried out using Comparative Molecular Field Analysis (CoMFA), aiming to deduce rational guidelines for the further structural modification of these lead compounds.



## 1. Introduction

Mitochondrial monoamine oxidases (MAOs, EC 1.4.3.4) are flavin-containing enzymes (FAD) that catalyze the oxidative deamination of neurotransmitters and exogenous arylalkylamines. In mammals, two different types of MAOs are present in most tissues, namely, MAO-A and MAO-B. MAO-A preferentially deaminates aromatic monoamines such as the neurotransmitters serotonin (5-HT), noradrenaline (NA), and adrenaline (A), while MAO-B mainly oxidizes α-phenylethylamines and benzylamine. Both isoforms act on dopamine (D) and tryptamine.[1]

These enzymes are tightly bound to the mitochondrial outer membrane, sharing about 70% amino acid identity. They also differ with respect to substrate specificity, sensitivity to inhibitors, and tissue distribution.

Although MAOs are widely distributed in various organs, most of the studies concerning their functional properties and involvement in pathological processes have been mainly focused on the central nervous system. In the periphery, MAO-A and MAO-B are differently expressed in a variety of tissues: MAO-A is predominant in heart, adipose tissue, and skin fibroblasts, MAO-B is the major form found in platelets and lymphocytes, whereas both isoenzymes are expressed in kidney and liver.[2] It has been recently identified an additional MAO mechanism which is involved in reactive oxygen species (ROS) production and the consequent induction of intracellular oxidative stress. Hydrogen peroxide ($H_2O_2$) is one of the reaction products generated by MAOs during substrate degradation. Except for the potential cytotoxic effect of $H_2O_2$ in nigral cells in Parkinson's disease, the cell events following MAO-dependent $H_2O_2$ production in physiological conditions are still

* Corresponding author. Tel.: +39 06 4991 3763; fax: +39 06 49913772.
*E-mail address:* daniela.secci@uniroma1.it (D. Secci).

0968-0896/$ - see front matter © 2010 Elsevier Ltd. All rights reserved.
doi:10.1016/j.bmc.2010.05.070

unknown. These findings, along with other results showing the important role of ROS generated by MAOs in heart, adipose tissue, macrophages, and skeletal muscle, pointed to the relevance also of peripheral MAOs in various pathological processes and their potentiality as pharmacological agents.[3]

The discovery of reversible and selective inhibitors has renewed the interest towards MAO enzymes as drug targets. In fact, irreversible and/or nonselective inhibitors showed shortcomings including cumulative effects, loss of selectivity after chronic treatment, and interaction with tyramine-containing foods (cheese-effect). Selective and reversible hMAO-A inhibitors (hMAO-AIs) are currently used in the treatment of depression and anxiety disorders, whereas hMAO-B inhibitors (hMAO-BIs) are used as adjuncts in the treatment of Parkinson's disease (PD). MAO-B predominates over MAO-A in the human brain especially after the 60th year of life, where hMAO-BIs have proven to be beneficial in prolonging the anti-Parkinsonian action of L-DOPA. hMAO-BIs, which decrease the rate of MAO-B catalyzed oxidative deamination and, consequently, the production of reactive oxygen species (ROS), might contribute to the treatment of other neurodegenerative diseases, such as Alzheimer's disease.[4–6]

The rational design of new agents targeted to MAOs could be based on the recent description of the crystal structure of human MAO-B and MAO-A with their corresponding inhibitors and aided with theoretical calculations.[7,8] The above studies elucidated some factors responsible for selectivity against the A and B isoforms, such as the lipophilicity of the inhibitor that is important for achieving effective binding to MAO-B, the presence of electron-rich aromatic moieties, typical of selective MAO-A inhibitors, and the role played by some amino acid residues in the active sites, such as Tyr326 for hMAO-B and Ile335 for hMAO-A.[9]

The aim of the present study was the identification of novel potent and selective hMAO inhibitors that could serve as potential lead molecules for drug discovery. An examination of the chemical structures of MAOIs of clinical interest (Fig. 1) and the analysis of patents dealing with new inhibitors[10] led us to identify some structural features that characterize these compounds: (i) a basic nitrogen atom, sometimes incorporated in an alicyclic ring and (ii) an electron-rich aromatic moiety that plays a pivotal role in the interaction with the biological target, as shown in recent QSAR studies.[11] The same structural features are found in dopamine, a MAO-A and MAO-B substrate.

In the past decade, we have reported several series of reversible and potent MAOIs,[12,13] some of which allowed the 2-thiazolylhydrazone nucleus to be identified as scaffold for promising hMAO-B selective inhibitors.[14] The cyclo-thiosemicarbazone moiety represents the pharmacophore portion. Docking studies suggest that the orientation of the two series, N1-thiocarbamoylpyrazolines and 2-thiazolylhydrazones, can be compared within the enzymatic active site as reported in Figure 2.

Furthermore, a large number of substituted hydrazines have been studied as MAO inhibitors and their specific mechanism of action was fully investigated.[15]

Substituents on the aromatic ring at C4 position of thiazole ring also influenced the activity, as shown by the introduction of several groups ($NO_2$, CN, $CH_3$, $OCH_3$) or halogens (F, Cl) in the *ortho* and *para* positions,[14] while the introduction of more steric hindered coumarin or naphthalene nuclei at C4 position of thiazole, led to a decreased hMAO inhibitory activity.[16] Different cycloaliphatic moieties, probed onto the C=N group, allowed us to systematically explore the steric influence of this substituent on the MAO inhibitor activity. In the past other authors have investigated some hydrazothiazoles as regards their potency as rat MAO inhibitors, and their thermotropic behavior in relation to the partition coefficient in lipidic membrane models, correlating a different binding of these inhibitors to the enzyme surface according to their electronic or lipophilic characteristics.[17]

Since our major goal was to identify novel lead compounds with hMAO inhibitory activity, in this paper we report on the synthesis, the biological properties, and 3D-QSAR studies of 4-aryl-2-thia-

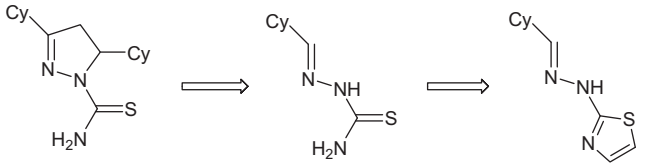


**Figure 2.** Conversion of N1-thiocarbamoyl-3,5-diaryl-4,5-dihydro-(1*H*)-pyrazole in cycloalkylidenhydrazothiazole derivative.

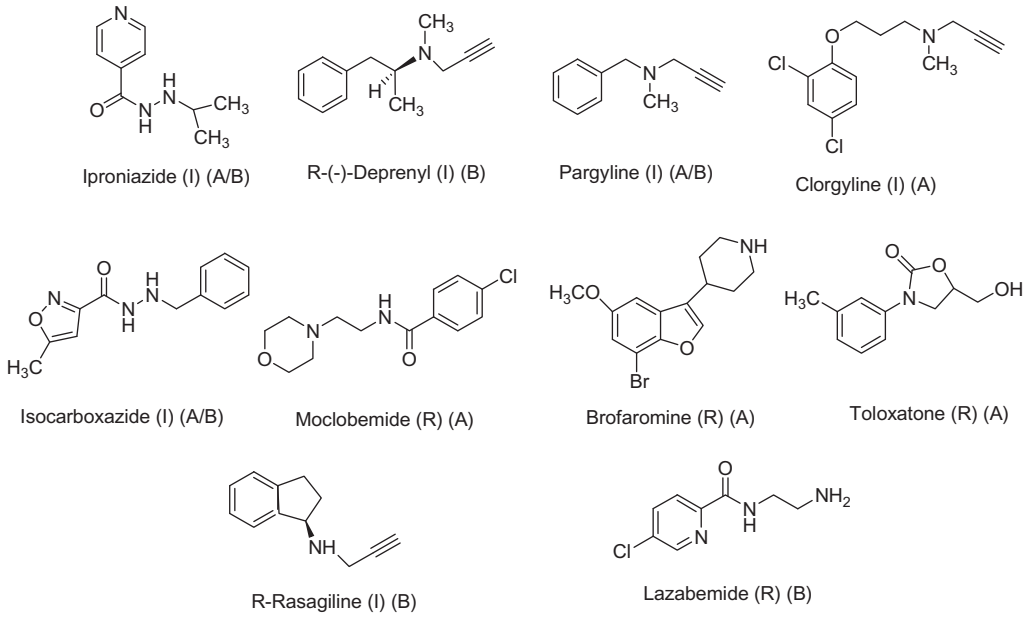


**Figure 1.** Irreversible (I), reversible (R), and/or selective hMAO-A and hMAO-B inhibitors (A and/or B).

zolylhydrazone derivatives (**1**–**45**) useful to assess a pharmacophore motif common to the active compounds.

## 2. Chemistry

All (4-aryl-thiazol-2-yl)hydrazone derivatives **1**–**45** were synthesized[14,16] in high yields (70–99%) as reported in Scheme 1 and listed in Table 1. Different carbonyl compounds reacted directly with thiosemicarbazide in ethanol or in 2-propanol with catalytic amounts of acetic acid, and the obtained thiosemicarbazones were subsequently converted in (4-aryl-thiazol-2-yl)hydrazones by Hantzsch reaction with 2- or 2,4-substituted α-bromo-acetophenones in the same solvent. α-Bromoacetophenones have been synthesized by direct halogenation of the corresponding acetophenones with bromine in chloroform.[18]

All the synthesized compounds were washed with petroleum ether, hexane or diethyl ether and, if necessary, purified by chromatography before characterization by spectroscopic methods (see Supplementary data).

## 3. Semipreparative HPLC enantioseparation

Owing to the presence of a stereogenic carbon on the cyclohexyl ring (**37**–**45**), some compounds exist as (*R*)- and (*S*)-enantiomers. The first step towards the investigation of the impact of absolute stereochemistry on the activity and selectivity was to isolate sufficient quantities of the enantiomers of four of the most active compounds to use in a parallel test in vitro. Our strategy was to synthesize quantitatively the racemic forms and successively resolve them by HPLC on polysaccharide-based chiral stationary phases (CPSs) on a semipreparative scale. A combined method based on chemical correlation, single-crystal X-ray diffraction, and enantioselective HPLC allowed us to assign the absolute configuration of the isolated enantiomers. Knowledge of the absolute configuration and in vitro biological activity of homochiral forms were needed in the in silico study of the interactions involving the receptor site. For the stereocontrolled synthesis of the pure enantiomers of compounds **39**, **41**, **44**, and **45**, we used the enantiopure forms of 2-methylcyclohexylidene thiosemicarbazone (2-MCET) as chiral synthon, on the basis of a previous study by us on the enantioseparation and configurational stability of this compound.[19] The racemic 2-MCET obtained in the first step of the reaction was separated by enantioselective HPLC on a semipreparative scale, and the isolated pure enantiomers were used for the second step. The absolute configuration of the chiral synthon was established by a single-crystal X-ray diffraction analysis. From the findings of the X-ray structure analysis, we could assign unambiguously the (*S*)-configuration to the C2 stereogenic center located on the cyclohexyl ring of the (+)-2-MCET enantiomer. Starting from the enantiopure forms of 2-MCET of known stereochemistry, we obtained enantioenriched forms of the target molecules with correlated chirality. The stereochemical course of the reaction was monitored by the same enantioselective HPLC system used for the semipreparative enantioseparation. The cyclization of the chiral synthon is stereoconservative as demonstrated by the high ee values (95–98%) of the obtained thiazoles. The assignment of the absolute configuration of the enantiomers of compounds **37**–**45** was determined by chemical correlation using as reference compound the chiral synthon 2-MCET.

## 4. Biological activity

The inhibitory activity of the test drugs (new compounds and five reference inhibitors) against hMAOs was evaluated using a general procedure previously described by us.[20] The potential inhibitory activity was investigated by measuring the effects of new derivatives on the production of hydrogen peroxide ($H_2O_2$) from *p*-tyramine (a common substrate for both hMAO-A and hMAO-B), using the Amplex Red MAO assay kit and microsomal MAO isoforms prepared from insect cells (BTI-TN-5B1-4) infected with recombinant baculovirus containing cDNA inserts for hMAO-A or hMAO-B (Table 1).

## 5. Reversibility and irreversibility experiments

To evaluate whether these derivatives acted as reversible or irreversible hMAO inhibitor, an effective centrifugation–ultrafiltration method (so-called repeated washing), previously described by us, was used for the most active and selective derivative **44**.[14] The data reported in Table 2 showed that this compound acted as an irreversible inhibitor against both isoforms (using the same $IC_{50}$ values reported in Table 1), because the percent enzymatic inhibition was constant after repeated washing as respect to *R*-(−)-deprenyl (irreversible inhibitor), but different with respect to Moclobemide (reversible inhibitor). These results displayed a strong and long-lasting interaction with the enzyme which could not restore its enzymatic activity in the presence of the inhibitor. In most cases, the irreversible inhibitors establish a covalent interaction with the active center of the enzyme.[21] However, not all irreversible inhibitors form covalent adducts with their enzyme targets but they may also act by other mechanisms. In fact, some reversible inhibitors bind so tightly to their target enzyme that they are essentially irreversible. These tight-binding inhibitors may show kinetics similar to covalent irreversible inhibitors. In these cases, some of these inhibitors rapidly bind to the enzyme in a low-affinity enzyme–inhibitor (EI) complex and this then undergoes a slower rearrangement to a very tightly bound EI* complex. This kinetic behavior is called slow-binding. This slow rearrangement after binding often involves a conformational change as the enzyme 'clamps down' around the inhibitor molecule.[22]

Also some MAO irreversible inhibitors (the so-called suicide inhibitors) act as a substrate for the target enzyme, which finally generates a new compound that irreversibly inhibits MAO activity. Therefore, the initial interaction of these inhibitors with MAO may

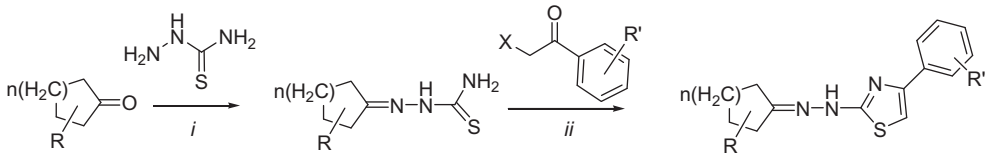


**1-45**

**Scheme 1.** Reagents and conditions: (i) $CH_3COOH$ (cat.), ethanol or 2-propanol, rt; (ii) ethanol, rt.

**Table 1**
Structures, biological activity ($IC_{50}$), and hMAO-B selectivity ratios for the inhibitory effects of tested compounds **1–45** and reference drugs on enzymatic activity of human recombinant MAO isoforms expressed in baculovirus infected cells

| Compd | R | R′ | hMAOA $IC_{50}$ (nM) | hMAOB $IC_{50}$ (nM) | Ratio |
|---|---|---|---|---|---|
| **1** | Cyclopentyl | H | 7883 ± 91* | 296 ± 7 | 27 |
| **2** | Cyclopentyl | 4-Cl | 7160 ± 640* | 262 ± 8 | 27 |
| **3** | Cyclopentyl | 4-F | 4436 ± 212* | 40 ± 0.9 | 111 |
| **4** | Cyclopentyl | 2,4-Cl | 54,507 ± 4123* | 284 ± 11 | 192 |
| **5** | Cyclopentyl | 2,4-F | 2318 ± 161* | 3 ± 0.2 | 773 |
| **6** | Cyclopentyl | 4-$CH_3$ | 2019 ± 74* | 134 ± 9 | 15 |
| **7** | Cyclopentyl | 4-$OCH_3$ | 1055 ± 42* | 164 ± 13 | 6 |
| **8** | Cyclopentyl | 4-$NO_2$ | 344 ± 22* | 94 ± 3 | 4 |
| **9** | Cyclopentyl | 4-CN | 644 ± 21* | 221 ± 2 | 3 |
| **10** | Cyclohexyl | H | 48,351 ± 1433* | 116 ± 5 | 417 |
| **11** | Cyclohexyl | 4-Cl | 2911 ± 171* | 211 ± 7 | 14 |
| **12** | Cyclohexyl | 4-F | 1752 ± 21* | 4 ± 0.2 | 438 |
| **13** | Cyclohexyl | 2,4-Cl | N.E. | 202 ± 16 | >495[b] |
| **14** | Cyclohexyl | 2,4-F | 45,754 ± 143* | 652 ± 22 | 70 |
| **15** | Cyclohexyl | 4-$CH_3$ | 23,731 ± 324* | 3689 ± 353 | 6 |
| **16** | Cyclohexyl | 4-$OCH_3$ | 7509 ± 213** | 11,956 ± 131 | 0.6 |
| **17** | Cyclohexyl | 4-$NO_2$ | 24,154 ± 824* | 86 ± 3 | 281 |
| **18** | Cyclohexyl | 4-CN | 4837 ± 183* | 53 ± 2 | 91 |
| **19** | 4-Methylcyclohexyl | H | 34,223 ± 1486* | 259 ± 8 | 132 |
| **20** | 4-Methylcyclohexyl | 4-Cl | 15,217 ± 355* | 2411 ± 30 | 6 |
| **21** | 4-Methylcyclohexyl | 4-F | 45,457 ± 3119* | 43 ± 1 | 1057 |
| **22** | 4-Methylcyclohexyl | 2,4-Cl | 81,485 ± 3766* | 9446 ± 352 | 9 |
| **23** | 4-Methylcyclohexyl | 2,4-F | 19,496 ± 1127* | 91 ± 0.8 | 214 |
| **24** | 4-Methylcyclohexyl | 4-$CH_3$ | 8109 ± 442** | 5477 ± 461 | 1.5 |
| **25** | 4-Methylcyclohexyl | 4-$OCH_3$ | 5763 ± 197* | 31,197 ± 1055 | 0.2 |
| **26** | 4-Methylcyclohexyl | 4-$NO_2$ | 20,882 ± 788* | 362 ± 16 | 58 |
| **27** | 4-Methylcyclohexyl | 4-CN | 6994 ± 351* | 61 ± 0.7 | 115 |
| **28** | Cycloheptyl | H | 14,851 ± 739* | 27 ± 0.6 | 550 |
| **29** | Cycloheptyl | 4-Cl | 6182 ± 173* | 477 ± 15 | 13 |
| **30** | Cycloheptyl | 4-F | 10,279 ± 812* | 4 ± 0.2 | 2570 |
| **31** | Cycloheptyl | 2,4-Cl | 59,280 ± 2845* | 940 ± 13 | 63 |
| **32** | Cycloheptyl | 2,4-F | 7229 ± 490* | 16 ± 0.4 | 452 |
| **33** | Cycloheptyl | 4-$CH_3$ | 9612 ± 716* | 920 ± 31 | 10 |
| **34** | Cycloheptyl | 4-$OCH_3$ | 3925 ± 84** | 5025 ± 160 | 0.8 |
| **35** | Cycloheptyl | 4-$NO_2$ | 17,853 ± 1026* | 11 ± 0.4 | 1623 |
| **36** | Cycloheptyl | 4-CN | 4327 ± 263* | 46 ± 2 | 94 |
| **37** | 2-Methylcyclohexyl | H | 41,236 ± 3962* | 711 ± 37 | 58 |
| **38** | 2-Methylcyclohexyl | 4-Cl | 35,220 ± 1813* | 13,126 ± 517 | 3 |
| **39** | 2-Methylcyclohexyl | 4-F | 43,556 ± 3611* | 204 ± 8 | 214 |
| (*S*)-**39** | 2-Methylcyclohexyl | 4-F | 4943 ± 92* | 47 ± 2 | 105 |
| (*R*)-**39** | 2-Methylcyclohexyl | 4-F | 3536 ± 125* | 22 ± 1 | 161 |
| **40** | 2-Methylcyclohexyl | 2,4-Cl | 44,705 ± 5234** | 26,811 ± 2745 | 2 |
| **41** | 2-Methylcyclohexyl | 2,4-F | 37,955 ± 3413* | 14 ± 0.3 | 2711 |
| (*S*)-**41** | 2-Methylcyclohexyl | 2,4-F | 4813 ± 35* | 36 ± 3 | 134 |
| (*R*)-**41** | 2-Methylcyclohexyl | 2,4-F | 6834 ± 148* | 30 ± 3 | 228 |
| **42** | 2-Methylcyclohexyl | 4-$CH_3$ | N.E. | 143 ± 9 | >699[b] |
| **43** | 2-Methylcyclohexyl | 4-$OCH_3$ | 2762 ± 171 | 2373 ± 145 | 1.2 |
| **44** | 2-Methylcyclohexyl | 4-$NO_2$ | N.E. | 32 ± 2 | >3125[b] |
| (*S*)-**44** | 2-Methylcyclohexyl | 4-$NO_2$ | 42,316 ± 2815* | 17 ± 0.9 | 2489 |
| (*R*)-**44** | 2-Methylcyclohexyl | 4-$NO_2$ | 43,953 ± 1087* | 10 ± 0.7 | 4395 |
| **45** | 2-Methylcyclohexyl | 4-CN | 31,034 ± 2446* | 26 ± 1 | 1194 |
| (*S*)-**45** | 2-Methylcyclohexyl | 4-CN | 7221 ± 563* | 63 ± 4 | 115 |
| (*R*)-**45** | 2-Methylcyclohexyl | 4-CN | 5507 ± 261* | 32 ± 2 | 172 |
| C | | | 5 ± 0.3* | 61,356 ± 1137 | 0.00008 |
| De | | | 67,250 ± 1025* | 20 ± 0.9 | 3363 |
| I | | | 6566 ± 763 | 7547 ± 361 | 0.9 |
| M | | | 361,382 ± 19,374 | N.E. | <0.4[a] |
| Is | | | N.E. | 18,754 ± 1242 | >5[b] |

C = clorgyline, De = *R*-(−)-deprenyl, I = iproniazid, M = moclobemide, Is = isatin. Ratio: hMAO-B selectivity index = $IC_{50\ (hMAO\text{-}A)}/IC_{50\ (hMAO\text{-}B)}$. Each $IC_{50}$ value is the mean ± S.E.M. from five experiments. Level of statistical significance: * $P < 0.01$ or ** $P < 0.05$ versus the corresponding $IC_{50}$ values obtained against hMAO-B, as determined by ANOVA/Dunnett's. N.E. = Inactive at 100 μM (highest concentration tested).

[a] Values obtained under the assumption that the corresponding $IC_{50}$ against hMAO-B is the highest concentration tested (1 mM).

[b] Value obtained under the assumption that the corresponding $IC_{50}$ against hMAO-A is the highest concentration tested (100 μM).

be different to the interaction obtained after several minutes of the enzyme-inhibitor complex formation. *R*-(−)-deprenyl, for example, first of all form a non-covalent complex with MAO as an initial, reversible step. The subsequent interaction of *R*-(−)-deprenyl with MAO leads to a reduction of the enzyme-bound flavin adenine dinucleotide, and concomitant oxidation of the inhibitor. This oxidized inhibitor then reacts with FAD at the N-5-position in a covalent manner.[23] The initial non-covalent binding to MAO has been also described for other MAO inhibitors.[24] Finally, it is possible that, in some cases of irreversible inhibition, a steric hindrance may drastically difficult the removal of the inhibitor from the enzymatic active center (although its interaction with this binding site is either very weak or reversible). Bearing in mind all the above considerations and taking into account that the docking studies

**Table 2**
Reversibility and irreversibility of hMAO inhibition of derivative **44** and reference inhibitors[a]

| Compd | % hMAO-A inhibition | | % hMAO-B inhibition | |
|---|---|---|---|---|
| | Before washing | After repeated washing | Before washing | After repeated washing |
| Moclobemide (500 μM) | 86.75 ± 4.34[a] | 10.26 ± 0.65 | | |
| **44** (100 μM) | 23.41 ± 1.62 | 26.61 ± 1.54 | | |
| (*S*)-**44** (100 μM) | 69.47 ± 3.76 | 71.47 ± 3.47 | | |
| (*R*)-**44** (100 μM) | 60.56 ± 2.98 | 58.43 ± 2.76 | | |
| *R*-(−)-Deprenyl (20 nM) | | | 48.67 ± 2.34[a] | 49.14 ± 2.80 |
| **44** (50 nM) | | | 58.65 ± 2.97 | 60.19 ± 3.26 |
| (*S*)-**44** (50 nM) | | | 74.32 ± 4.14 | 79.26 ± 4.32 |
| (*R*)-**44** (50 nM) | | | 77.83 ± 3.89 | 81.63 ± 4.25 |

Each value is the mean ± S.E.M. from five experiments ($n = 5$).
[a] Level of statistical significance: $P < 0.01$ versus the corresponding % hMAO-A or hMAO-B inhibition before washing, as determined by ANOVA/Dunnett's.

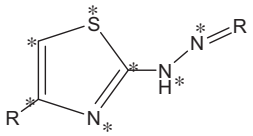

**Scheme 2.** Substructure of the common core of the molecules used for rigid fitting to the template.

make only a theoretical prediction of the initial possible interaction inhibitor-enzyme, the results obtained in these docking studies and in the reversibility experiments may be different.

## 6. Molecular modeling

The CoMFA[25] study was performed using Sybyl v. 7.2.[26] A well-defined training set of 36 compounds was collected and used for model generation. Compounds **37**–**45** show a chiral center as well a *E*/*Z* double bond configuration. As the in vitro activity for all respective configurations is not available and in order to assure high quality data for the model generation, these configurations were excluded for such compounds. Derivatives **39**, **41**, **44**, and **45**, whose activity data of separated enantiomeric forms are available, were employed as a test set for the model validation. Knowing that the alignment plays a fundamental role in the COMFA studies, different alignments have been used to define the best one for our set of compounds. First of all, we applied substructure-based alignment. All the molecules were submitted to full geometry optimization by molecular mechanics using the standard Tripos force field[27] with a distance dependent dielectric ($\varepsilon = 1$) and Powell conjugate gradient algorithm[28] (convergence criterion of 0.001 kcal/mol Å). Atomic charges were calculated using the Gasteiger–Hückel method.[29] Compound **30** was used as template, and the moiety considered for the alignment is shown with asterisked atoms in the Scheme 2.

The aligned molecules were included into a sufficiently large box considering a grid spacing equal to 2.0 Å. The steric and electrostatic fields were computed using an $sp^3$ C-atom with explicit electrostatic charge fixed to +1. Partial least square (PLS) was adopted for deriving the linear equation from the resulting field matrix using the cross-validate leave-one-out (LOO) method. Minimum sigma equal to 2 kcal/mol was applied in order to decrease noise. Table 3 shows the calculated CoMFA statistical parameters.

The cross-validated analysis, obtaining $q^2$ greater than 0.3, was considered for model generation, as with this $q^2$ cut-off the probability of chance correlation is lower than 5%.[25] PLS analysis was processed without validation to derive the square of no-cross-validated correlated coefficient ($r^2$). The number of optimum components (NOC) taken into account for the $r^2$ calculation was assessed by previous cross-validated analysis. This allows to de-noise data and to avoid over-fitting. For all further analysis the same setting described above were applied. The most important requirement for CoMFA studies is that the 3D structures to be analyzed are aligned according to a suitable conformational template, which is assumed to be the 'bioactive' conformation. The pharmacophore-based alignment represents another commonly used approach, in particular when the substructure-based alignment method fails.[30–32] We generated the pharmacophore models by means of the HipHop algorithm, as included in Catalyst package.[33] HipHop generates hypotheses which have common feature. Compounds **30** (principal2), **12**, **5**, **35**, **21**, **19** (principal1) were chosen for the model generation. The pharmacophores differing from direction of projection points were discarded, the remaining models were used for the alignment procedure. Once the aligned compounds were imported in Sybyl, their electrostatic charge distribution was computed using the Gasteiger–Hückel method. Only the statistical values of the best pharmacophore-based alignment are shown in Table 3.

However the models based on this alignment exhibited only minor improvements from the previous one. Therefore we decided to apply a receptor-based alignment using the docking program GLIDE,[34] as we found this approach to work reliably in our previous study on the same target[13b] and in other studies reported in literature.[35,36] The conformational properties of compounds have been investigated by Monte Carlo (MC) search applying 5000 iterations to all rotatable bonds. Each generated structure has been optimized with at least 2000 interactions of the Polak Ribiere Conjugate Gradient algorithm using MMFFs force field and the implicit solvation model GB/SA water, as implemented in MacroModel

**Table 3**
Statistical results of different models derived from the training set molecules using different alignments

| Model | $q^2$ | NOC | SEP | $r^2$ | SEE | $F$ | Steric% |
|---|---|---|---|---|---|---|---|
| Substructure based MAO-A | 0.449 | 5 | 0.473 | 0.752 | 0.317 | 18227 | 57 |
| Substructure based MAO-B | 0.356 | 4 | 0.829 | 0.678 | 0.586 | 16286 | 62 |
| Pharmacophore based MAO-A | 0.352 | 4 | 0.504 | 0.768 | 0.302 | 25603 | 50 |
| Pharmacophore based MAO-B | 0.444 | 4 | 0.770 | 0.790 | 0.474 | 29081 | 51 |
| Receptor based MAO-A | 0.811 | 4 | 0.273 | 0.961 | 0.125 | 188759 | 40 |
| Receptor based MAO-B | 0.831 | 4 | 0.224 | 0.948 | 0.135 | 141468 | 47 |

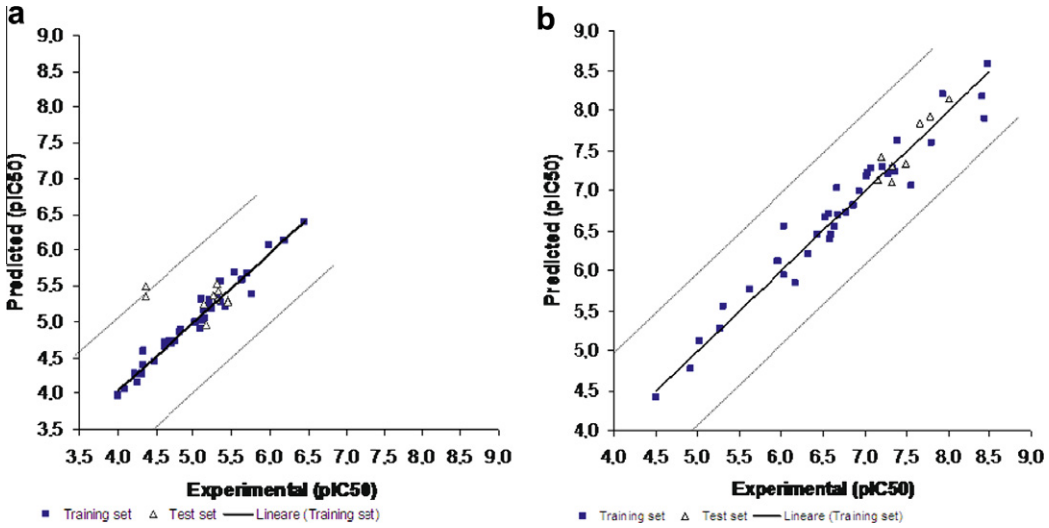


**Figure 3.** Correlation between experimental versus predicted activities of training and test set of MAO-A (a) and MAO-B (b). In addition, beside the line of ideal correlation, dotted lines are given, which indicated deviation from the actual $pIC_{50}$ by 1 logarithmic unit.

**Table 4**
Comparison between experimental (exp) and predicted (pred) $pIC_{50}$ by CoMFA models obtained with structure-based alignment

| Compd | MAO-A | | | MAO-B | | |
|---|---|---|---|---|---|---|
| | Config | $pIC_{50}$ exp | $pIC_{50}$ pred | Config | $pIC_{50}$ exp | $pIC_{50}$ pred |
| *Training set* | | | | | | |
| **1** | | 5.10 | 5.31 | | 6.53 | 6.67 |
| **2** | | 5.14 | 5.16 | | 6.58 | 6.71 |
| **3** | | 5.35 | 5.57 | | 7.39 | 7.63 |
| **4** | | 4.26 | 4.15 | | 6.60 | 6.45 |
| **5** | | 5.64 | 5.59 | | 8.49 | 8.58 |
| **6** | | 5.70 | 5.67 | | 6.87 | 6.81 |
| **7** | | 5.98 | 6.08 | | 6.79 | 6.72 |
| **8** | | 6.46 | 6.40 | | 7.02 | 7.17 |
| **9** | | 6.19 | 6.14 | | 6.65 | 6.55 |
| **10** | | 4.31 | 4.28 | | 6.93 | 6.99 |
| **11** | | 5.54 | 5.69 | | 6.67 | 7.03 |
| **12** | | 5.76 | 5.39 | | 8.42 | 8.18 |
| **13** | | 4.00 | 3.97 | | 6.69 | 6.69 |
| **14** | | 4.34 | 4.39 | | 6.18 | 5.84 |
| **15** | | 4.62 | 4.71 | | 5.96 | 6.12 |
| **16** | | 5.12 | 5.02 | | 4.92 | 4.77 |
| **17** | | 4.62 | 4.66 | | 7.07 | 7.28 |
| **18** | | 5.32 | 5.32 | | 7.28 | 7.21 |
| **19** | | 4.47 | 4.44 | | 6.59 | 6.39 |
| **20** | | 4.82 | 4.86 | | 5.62 | 5.76 |
| **21** | | 4.34 | 4.60 | | 7.36 | 7.23 |
| **22** | | 4.09 | 4.06 | | 5.02 | 5.12 |
| **23** | | 4.71 | 4.69 | | 7.04 | 7.22 |
| **24** | | 5.09 | 4.92 | | 5.26 | 5.28 |
| **25** | | 5.24 | 5.19 | | 4.50 | 4.42 |
| **26** | | 4.68 | 4.73 | | 6.44 | 6.45 |
| **27** | | 5.15 | 5.05 | | 7.21 | 7.29 |
| **28** | | 4.83 | 4.89 | | 7.56 | 7.06 |
| **29** | | 5.21 | 5.30 | | 6.32 | 6.21 |
| **30** | | 4.99 | 5.26 | | 8.45 | 7.90 |
| **31** | | 4.23 | 4.28 | | 6.03 | 5.94 |
| **32** | | 5.14 | 5.16 | | 7.79 | 7.60 |
| **33** | | 5.02 | 5.00 | | 6.04 | 6.55 |
| **34** | | 5.41 | 5.21 | | 5.30 | 5.55 |
| **35** | | 4.75 | 4.73 | | 7.94 | 8.21 |
| **36** | | 5.36 | 5.28 | | 7.34 | 7.28 |
| *Test set* | | | | | | |
| **(S)-39** | *E* | 5.30 | 5.29 | *Z* | 7.32 | 7.30 |
| **(R)-39** | *E* | 5.45 | 5.32 | *E* | 7.66 | 7.25 |
| **(S)-41** | *E* | 5.32 | 5.43 | *E* | 7.18 | 7.14 |
| **(R)-41** | *Z* | 5.16 | 4.95 | *E* | 7.32 | 7.10 |
| **(S)-44** | *E* | 4.37 | 5.49 | *Z* | 7.78 | 7.93 |
| **(R)-44** | *E* | 4.36 | 5.35 | *Z* | 8.00 | 8.15 |
| **(S)-45** | *E* | 5.14 | 5.24 | *E* | 7.20 | 7.42 |
| **(R)-45** | *Z* | 5.26 | 5.36 | *E* | 7.49 | 7.34 |

v.7.2.[37] All MC minimum energy conformers were submitted to rigid docking using GLIDE. PDB structures 2BXR[38] and 1GOS[39] were used as human MAO-A and MAO-B target structures, respectively. A box of about 110 k Å$^3$ centered onto the N5 FAD atom was defined as binding site in GLIDE. For each compound, the ten best docked poses were considered for the receptor-based alignment. Starting from the highest ranked structure, the pose obtaining the best $q^2$ value was chosen for the alignment.[40] The Figure 3 depicts the plot of the experimental activities versus the predicted ones; the corresponding values are reported in Table 4, respectively.

In order to investigate the robustness of our models, a group cross-validation (10 groups, 20 times) was processed. The high average $q^2$ (Table 5) corroborates the stability of the models. Bootstrapping procedure (100 runs) was considered to exclude the risk of chance correlation.[41] Also in this case, the high value of $q^2$ and the minimal standard deviation confirmed the robustness of these models.

Furthermore, the predictive capability of our models was evaluated with the test set compounds: 10 conformers of each compound, obtained from the docking studies, were considered; the one with the highest predicted activity was defined the putative bioactive conformation. All *R*/*S* and *E*/*Z* isomers of **39**, **41**, **44**, and **45**, have been taken into account. As reported in Table 4 and Figure 3 due to the possible *E*/*Z* interconversion at room temperature, suggested by ab initio calculation,[14b] and considering that the respective predicted activities of both *E* and *Z* configurations are very similar, only one value was considered for these isomers. The activity of the test set compounds was accurately predicted by both models.

## 7. Results and discussion

CoMFA results of the best models obtained were analysed in order to highlight further modification onto the thiazole scaffold.

**Table 5**
Validation of the stability of the receptor-based models

| Model | Group cross-validation | Bootstrapping | |
|---|---|---|---|
| | Average $q^2$ | Average $q^2$ | Standard deviation $q^2$ |
| Model MAOA | 0.732 | 0.949 | 0.019 |
| Model MAOB | 0.805 | 0.952 | 0.019 |

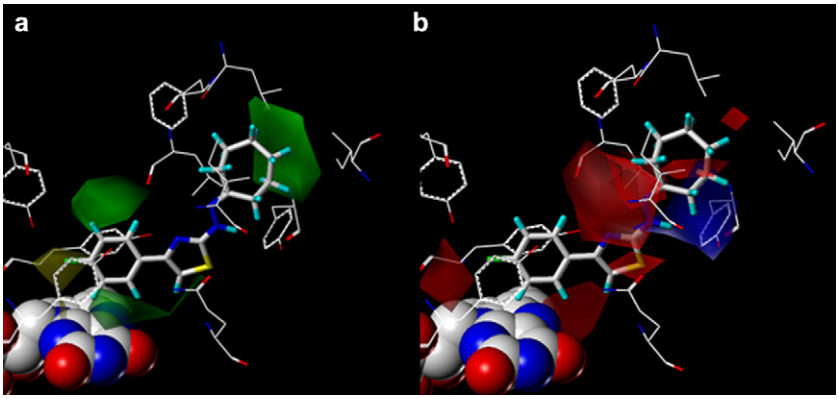


**Figure 4.** Contour 'stdev x coeff' plot of (a) steric and (b) electrostatic properties for the CoMFA model for MAO-B in combination with exemplary compound **30** in capped sticks and FAD in space fill style. Green contours indicate regions where an increase in steric bulk will enhance the activity; yellow contour indicates steric bulk unfavorable area. Blue and red contours show regions of desirable positive and negative electrostatic interactions, respectively.

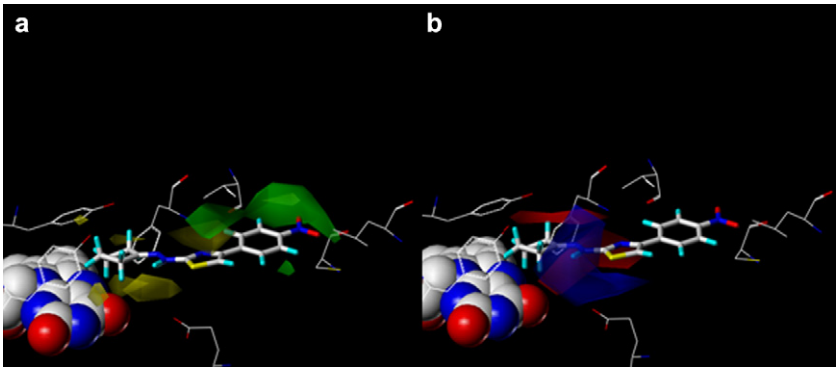


**Figure 5.** Contour 'stdev x coeff' plot of (a) steric and (b) electrostatic properties for the CoMFA model for MAO-A in combination with exemplary compound **8** in capped sticks and FAD in space fill style. Green contours indicate regions where an increase in steric bulk will enhance the activity; yellow contour indicates steric bulk unfavorable area. Blue and red contours show regions of desirable positive and negative electrostatic interactions, respectively.

The CoMFA contour map of MAO-B steric contribution, overlapping compound **30**, is depicted in Figure 4a.

A large green contour around the alicyclic portion and *ortho* position of phenyl ring, suggests that substitution with a more steric bulky groups at these positions may enhance activity. The small yellow contour map surrounding the phenyl ring indicates that occupancy of this sterically unfavorable area would have a detrimental effect on the inhibitory activity, for example, in **16** and **25** the substitution of fluorine with bulkier methoxy group leads to lower activity compounds. The electrostatic CoMFA field is shown in Figure 4b. Here, a small red contour map around the phenyl ring *para* position remarks the relevance of an electronegative group at this location for inhibitory activity.

Such a suggestion is consistent with higher activity of **3**, **12**, **21**, and **30**, showing a fluorine, with respect to, for example, **15** and **33**, which have a methyl group. At the same time, the close yellow map suggests that electronegative groups should not be too bulky. Another red contour map is placed in correspondence of the hydrazo group, while a large blue contour map is wrapped around the NH-position of this moiety. The first area indicates that an hydrogen bond acceptor is important at this position and the blue one remarks the key role played by the hydrogen bond donor NH.

The docking experiment on MAO-A revealed that most of the compounds showed orientation of the alicyclic part towards the cofactor as it is shown in Figure 5. The difference of the putative binding mode in the two isoforms could be due to shape and volume differences of the substrate cavities. The MAO-A isoform presents a large substrate cavity, while the MAO-B substrate cavity is characterized by a narrow access cavity that precedes a larger one which accommodates bigger compounds able to go through the two cavities. This could explain the higher inhibitory activity on MAO-B of this series of compounds. The analysis of the corresponding maps for MAO-A (Fig. 5) confirms the relevance of the hydrazo group for the MAO recognition.

The green contour map suggests that substitution with bulky groups at the phenyl ring would lead towards MAO-A selective inhibitors, while, the substitution with bulky groups in correspondence of alicyclic portion does not seem favorable for MAO-A inhibitory activity since small yellow areas are surrounding this position. As above mentioned, this substitution would probably enhance the activity towards MAO-B consequently increasing the selectivity for B isoform. These considerations lead us to consider appropriate modifications on this scaffold. Though some portions seem to be essential, the maps clearly indicate some possibilities for the improvement of activity and selectivity.

The aim of this study was to rationalize the structure–activity relationships of these new hMAO inhibitors by deriving a suitable selectivity model. The receptor-guided alignment allowed us to obtain the most accurate model. The information deduced will be taken into account for structural modification on this scaffold.

## Acknowledgments

This work was supported by MURST (Italy), Ministerio de Sanidad y Consumo (Spain; FISS PI061537) and Xunta de Galicia (Spain; INCITE07PXI203039ES, INCITE08E1R203054ES, and 08CSA019 203PR).

## Supplementary data

Supplementary data associated with this article can be found, in the online version, at doi:10.1016/j.bmc.2010.05.070.

## References and notes


1. (a) Edmondson, D. E.; Mattevi, A.; Binda, C.; Li, M.; Hubálek, F. *Curr. Med. Chem.* **2004**, *11*, 1983; (b) Edmondson, D. E.; De Colibus, L.; Binda, C.; Li, M.; Mattevi, A. *J. Neural Transm.* **2007**, *114*, 703; (c) Edmondson, D. E.; Binda, C.; Wang, J.; Upadhayay, A. K.; Mattevi, A. *Biochemistry* **2009**, *48*, 4220.
2. (a) Shih, J. C.; Chen, K.; Ridd, M. J. *Annu. Rev. Neurosci.* **1999**, *22*, 197; (b) Shih, J. C.; Chen, K. *Curr. Med. Chem.* **2004**, *11*, 1995.
3. (a) Sayre, L. M.; Perry, G.; Smith, M. A. *Chem. Res. Toxicol.* **2008**, *21*, 172; (b) Blandini, F. *CNS Drug Rev.* **2005**, *11*, 183.
4. (a) Youdim, M. B. H.; Edmondson, D. E.; Tipton, K. F. *Nat. Rev.* **2006**, *7*, 295; (b) Bortolato, M.; Chen, K.; Shih, J. C. *Adv. Drug Deliv. Rev.* **2008**, *60*, 1527; (c) Riederer, P.; Lachenmayer, L.; Laux, G. *Curr. Med. Chem.* **2004**, *11*, 2033.
5. (a) Da Prada, M.; Kettler, R.; Keller, H. H.; Cesura, A. M.; Richards, J. G.; Saura Marti, J.; Muggli-Maniglio, D.; Wyss, P. C.; Kyburz, E.; Imhof, R. *J. Neural Transm. Suppl.* **1990**, *29*, 279; (b) Guay, D. R. *Am. J. Geriatr. Pharmacother.* **2006**, *4*, 330; (c) Mellick, G. D.; Buchanan, D. D.; McCann, S. J.; James, K. M.; Johnson, A. G.; Davis, D. R.; Liyou, N.; Chan, D.; Le Couteur, D. G. *Mov. Disord.* **1999**, *14*, 219; (d) Drukarch, B.; Muiswinkel, F. L. *Biochem. Pharmacol.* **2000**, *59*, 1023.
6. Carreiras, M. C.; Marco, J. L. *Curr. Pharm. Des.* **2004**, *10*, 3167.
7. Son, S. Y.; Ma, J.; Kondou, Y.; Yoshimura, M.; Yamashita, E.; Tsukihara, T. *Proc. Natl. Acad. Sci. U.S.A.* **2008**, *105*, 5739. Data deposition: www.pdb.org (PDB ID code 2Z5X).
8. Hubálek, F.; Binda, C.; Khalil, A.; Li, M.; Mattevi, A.; Castagnoli, N.; Edmondson, D. E. *J. Biol. Chem.* **2005**, *280*, 15761. Data deposition: www.pdb.org (PDB ID code 2BK3).
9. Li, M.; Binda, C.; Mattevi, A.; Edmondson, D. E. *Biochemistry* **2006**, *45*, 4775.
10. Bolasco, A.; Fioravanti, R.; Carradori, S. *Expert Opin. Ther. Patents* **2005**, *15*, 1763.
11. Wouters, J. *Curr. Med. Chem.* **1998**, *5*, 137.
12. (a) Chimenti, F.; Secci, D.; Bolasco, A.; Chimenti, P.; Granese, A.; Befani, O.; Turini, P.; Alcaro, S.; Ortuso, F. *Bioorg. Med. Chem. Lett.* **2004**, *14*, 3697; (b) Chimenti, F.; Secci, D.; Bolasco, A.; Chimenti, P.; Granese, A.; Carradori, S.; Befani, O.; Turini, P.; Alcaro, S.; Ortuso, F. *Bioorg. Med. Chem. Lett.* **2006**, *16*, 4135; (c) Chimenti, F.; Secci, D.; Bolasco, A.; Chimenti, P.; Bizzarri, B.; Granese, A.; Carradori, S.; Yáñez, M.; Orallo, F.; Alcaro, S.; Ortuso, F. *J. Med. Chem.* **2009**, *52*, 1935.
13. (a) Chimenti, F.; Maccioni, E.; Secci, D.; Bolasco, A.; Chimenti, P.; Granese, A.; Befani, O.; Turini, P.; Alcaro, S.; Ortuso, F.; Cirilli, R.; La Torre, F.; Cardia, M. C.; Distinto, S. *J. Med. Chem.* **2005**, *48*, 7113; (b) Chimenti, F.; Bolasco, A.; Manna, F.; Secci, D.; Chimenti, P.; Granese, A.; Befani, O.; Turini, P.; Cirilli, R.; La Torre, F.; Alcaro, S.; Ortuso, F.; Langer, T. *Curr. Med. Chem.* **2006**, *13*, 1411; (c) Chimenti, F.; Carradori, S.; Secci, D.; Bolasco, A.; Bizzarri, B.; Chimenti, P.; Granese, A.; Yáñez, M.; Orallo, F. *Eur. J. Med. Chem.* **2010**, *45*, 800.
14. (a) Chimenti, F.; Maccioni, E.; Secci, D.; Bolasco, A.; Chimenti, P.; Granese, A.; Befani, O.; Turini, P.; Alcaro, S.; Ortuso, F.; Cardia, M. C.; Distinto, S. *J. Med. Chem.* **2007**, *50*, 707; (b) Chimenti, F.; Maccioni, E.; Secci, D.; Bolasco, A.; Chimenti, P.; Granese, A.; Carradori, S.; Alcaro, S.; Ortuso, F.; Yáñez, M.; Orallo, F.; Cirilli, R.; Ferretti, R.; La Torre, F. *J. Med. Chem.* **2008**, *51*, 4874.
15. (a) Tipton, K. F. *Biochem. J.* **1972**, *128*, 913; (b) Dar, A.; Khan, K. M.; Ateeq, H. S.; Khan, S.; Rahat, S.; Perveen, S.; Supuran, C. T. *J. Enzyme Inhib. Med. Chem.* **2005**, *20*, 269; (c) Binda, C.; Wang, J.; Li, M.; Hubálek, F.; Mattevi, A.; Edmondson, D. E. *Biochemistry* **2008**, *47*, 5616.
16. (a) Chimenti, F.; Carradori, S.; Secci, D.; Bolasco, A.; Chimenti, P.; Granese, A.; Bizzarri, B. *J. Heterocycl. Chem.* **2009**, *46*, 575; (b) Chimenti, F.; Secci, D.; Bolasco, A.; Chimenti, P.; Granese, A.; Carradori, S.; D'Ascenzio, M.; Yáñez, M.; Orallo, F. *Med. Chem. Commun.* **2010**. doi:10.1039/c0md00014K.
17. (a) Raciti, G.; Mazzone, P.; Raudino, A.; Mazzone, G.; Cambria, A. *Bioorg. Med. Chem.* **1995**, *3*, 1485; (b) Castelli, F.; Cambria, M. T.; Mazzone, P.; Pignatello, R. *Thermochim. Acta* **1997**, *302*, 143; (c) Cambria, A.; Raudino, A.; Geronikaki, A.; Buemi, G.; Raciti, G.; Mazzone, P.; Guccione, S.; Ragusa, S. *J. Enzyme Inhib.* **1999**, *14*, 307.
18. Pearson, D. I.; Poper, H. W.; Hargrove, W. E. *Org. Synth.* **1973**, *5*, 117.
19. Cirilli, R.; Ferretti, R.; La Torre, F.; Secci, D.; Bolasco, A.; Carradori, S.; Pierini, M. *J. Chromatogr., A* **2007**, *1172*, 160.
20. Yáñez, M.; Fraiz, N.; Cano, E.; Orallo, F. *Biochem. Biophys. Res. Commun.* **2006**, *344*, 688.
21. Tipton, K. F.; Boyce, S.; O'Sullivan, J.; Davey, G. P.; Healy, J. *Curr. Med. Chem.* **2004**, *11*, 1965.
22. Szedlacsek, S. E.; Duggleby, R. G. *Methods Enzymol.* **1995**, *249*, 144.
23. Gerlach, M.; Riederer, P.; Youdim, M. B. H. *Eur. J. Pharmacol.* **1992**, *226*, 97.
24. O'Brien, E. M.; Tipton, K. F.; Meroni, M.; Dostert, P. *J. Neural Transm. Suppl.* **1994**, *41*, 295.
25. Clark, M.; Cramer, R. D., III; Jones, D. M.; Patterson, D. E.; Simeroth, P. E. *Tetrahedron Comput. Methodol.* **1990**, *3*, 47.
26. Sybyl7.2, Tripos, St Louis, Missouri, USA.
27. Clark, M.; Cramer, R. D., III; Van Opdenbosch, N. *J. Comput. Chem.* **2004**, *10*, 982.
28. Powell, M. J. D. *Math. Prog.* **1977**, *12*, 241.
29. Gasteiger, J.; Marsili, M. *Tetrahedron* **1980**, *36*, 3219.
30. Langer, T.; Hoffmann, R. D. *J. Chem. Inf. Comput. Sci.* **1998**, *38*, 325.
31. Ryu, C.-K.; Lee, Y.; Park, S.-g.; You, H.-J.; Lee, R.-Y.; Lee, S.-Y.; Choi, S. *Bioorg. Med. Chem.* **2008**, *16*, 9772.
32. Chaudhaery, S. S.; Roy, K. K.; Saxena, A. K. *J. Chem. Inf. Model.* **2009**, *49*, 1590.
33. Catalyst 4.11, Accelrys, San Diego, CA, USA.
34. GLIDE, Schrodinger Inc, Portland, OR.
35. Clark, R. *J. Comput. Aided Mol. Des.* **2008**, *22*, 507.
36. Nicolotti, O.; Miscioscia, T. F.; Carotti, A.; Leonetti, F.; Carotti, A. *J. Chem. Inf. Model.* **2008**, *48*, 1211.
37. Macromodel,, Schrodinger Inc, Portland, OR.
38. De Colibus, L.; Li, M.; Binda, C.; Lustig, A.; Edmondson, E. D.; Mattevi, A. *Proc. Natl. Acad. Sci. U.S.A.* **2005**, *102*, 12684. Data deposition: www.pdb.org (PDB ID code 2BXR, 2BXS, and 2BYB).
39. Binda, C.; Newton-Vinson, P.; Hubálek, F.; Edmondson, D. E.; Mattevi, A. *Nat. Struct. Biol.* **2002**, *9*, 22. Data deposition: www.pdb.org (PDB ID code 1GOS).
40. Gamper, A. M.; Winger, R. H.; Liedl, K. R.; Sotriffer, C. A.; Varga, J. M.; Kroemer, R. T.; Rode, B. M. *J. Med. Chem.* **1996**, *39*, 3882.
41. Cramer, R. D.; Bunce, J. D.; Patterson, D. E.; Frank, I. E. *Quant. Struct.-Act. Relat.* **1988**, *7*, 18.